A Multi-State Model for Transmission System Resilience Enhancement Against Short-Circuit Faults Caused by Extreme Weather Events

Chao Guo, Chengjin Ye, Yi Ding, *Member, IEEE*, and Peng Wang, *Fellow, IEEE*

***Abstract*—Due to global climate change, the effect of extreme weather on power systems has attracted extensive attention. In the prior-art grid resilience studies, the hurricanes or wildfires are mainly defended in terms of expected line damages, while they are prone to trigger short-circuit fault (SCF) evolved with dynamic influence in reality. In this paper, a fragile model is developed to evaluate the nodal SCF probability considering the insulation aging of equipment and extreme weather condition. Then, a response framework for extreme weather events is developed for a transmission system to defend the cascading impacts of expected SCFs. Specifically, switches are shifted to restrain the out-of-range short-circuit currents (SCCs) so that to ensure the SCFs can be removed by circuit breakers, generation rescheduling and load shedding are arranged to maintain the post-fault system transient stability. The above measures are optimized simultaneously by an integrated Mixed-Integer Nonlinear Programming (MINLP). Considering the error or uncertainty of weather event forecasts, a multi-state model is established to provide the most cost-effective grid resilience enhancement scheme, in which the expected urgent adaptions of the initial scheme subject to weather state transition is included in the overall cost. The proposed model and techniques are validated using the IEEE 39-bus New-England test system and realistic meteorological data.**

***Index Terms*—Resilience, extreme weather, short-circuit fault, short-circuit current, transient stability, multi-state.**

I. Introduction

EXTREME weather events such as hurricanes and wildfires are becoming more frequent than ever, which greatly threatens the secure and reliable operation of power systems. In the U.S, between 2003 and 2012, roughly 679 power outages (each affecting at least 50000 customers) occurred due to weather events [1]. A resilient power system is supposed to be fault-tolerant with the ability to withstand and rapidly recover from extraordinary events [1], [2].

Manuscript received June 6, 2020; revised September 26, 2020 and November 24, 2020; accepted December 6, 2020. Date of publication December 10, 2020; date of current version July 23, 2021. The work was supported by the China NSFC under Grant 51807173. Paper no. TPWRD-00842-2020. *(Corresponding author: Chengjin Ye.)*

Chao Guo, Chengjin Ye, and Yi Ding are with the College of Electrical Engineering, Zhejiang University, Hangzhou 310027, China (e-mail: 11710014@zju.edu.cn; yechenjing@zju.edu.cn; yiding@zju.edu.cn).

Peng Wang is with the Electrical and Electronic Engineering School, School of Nanyang Technological University, Singapore 639798, Singapore (e-mail: epwang@ntu.edu.sg).

Color versions of one or more figures in this article are available at https://doi.org/10.1109/TPWRD.2020.3043938

Digital Object Identifier 10.1109/TPWRD.2020.3043938

Enhancing grid resilience against extreme weather events has been a key task of smart grid development [3]. However, the prior-art researches mostly focused on expected line damages caused by hurricanes or wildfires [4]–[6]. Consequently, power systems can only be guaranteed to be resilient against simple fault type. However, many contingencies triggered by extreme weather events are evolved with short-circuit faults (SCFs). For instance, it is reported that the massive power blackout in Brazil on 10th November 2009 resulted from three consecutive SCFs on the 765kV Itabera-Ivaipora line [7]. After the SCFs, the corresponding fault lines were cut off through circuit breakers. Over 3100 MW generation capacities of the Itaipu hydropower plant were curtailed. Subsequently, the power system oscillated and a blackout occurred, during which about 40% loads of the Brazil grid were lost. Generally, SCFs in power systems are caused by various factors such as insulation aging or external force, the occurrence probability of which is relatively low but grows significantly under extreme weather conditions. For instance, in hurricanes, the torrential rain tends to cause SCFs at cable connections with damaged insulations, and the strong winds may blow down trees and cause SCFs for overhead lines [8]. The evaluation of the SCF rate as well as its increasing mechanism with subject to extreme weather events has not been well studied.

SCFs exhibit a typical cascading impact on power systems. Specifically, after a SCF, relay protection isolates the fault through circuit breakers and restores the electricity via a reclosing, as a precondition of which, SCC is required to be restrained within the limit of breakers. The out-of-range SCC fails the fault isolation and may lead to sustained developing voltage drop or branch overload, which may further result in serious cascading failures or even blackouts. Therefore, the limitation of SCC should be considered in the response framework against extreme weather events for transmission systems. Common SCC limiting strategies include the deployment of fault current limiters (FCLs) [9], [10], switch shifting of lines [11], or bus splitting [12]. Some mixed-integer nonlinear programming (MINLP) or heuristic methods such as Genetic Algorithms (GA) [13], have been reported to be feasible for SCC limiting measure configuration.

Additionally, SCFs are prone to result in consequences such as sub-synchronous unit step-out and under-frequency load shedding. Due to the rapid increase of load and market deregulation, power systems operate closer to the stability boundaries. Therefore, besides the out-of-range SCC limitation, another

fundamental task for the power system to resist SCFs is transient stability maintenance. Fortunately, the transient stability constrained optimal power flow (TSCOPF) has been exploited to determine the cost-optimal generation rescheduling scheme for transient stability enhancement. A combined numerical discretization with the Interior Point Method (CNDIPM) [14] has been adopted as a mainstream solution for TSCOPF problems.

Generally, the prior-art SCC limiting measures and TSCOPF actions are implemented separately in different spatial and temporal scenes. As a consequence, under the obtained solutions, the corrected power system is not capable to resist the cascading effects of SCF triggered by the extreme weather event.

Furthermore, as aforementioned, the disturbance of extreme weather events on power system is indeed probable. In the Numerical Atmosphere Simulation (NAS) [15] framework, a set of conservation equations are numerically solved considering air parameters such as mass, momentum, and heat, and then reveals the forecasted path and strength of the weather event, which may be multi-solution and not exactly precise. In the prior-art grid resilience studies, robust optimization methods in a min-max-min framework have been widely utilized to provide the optimal hardening or emergency power supply actions for power systems against the most severe fault scenario [16]–[18]. Consequently, the low probability or rarity of the most severe fault leads to a relatively excessive cost and makes the suggested hurricane or wildfire defending strategy hard to be accepted by the benefit-oriented grid operators.

In this paper, the cascading impact of SCFs on power systems is investigated in terms of excessive SCC magnitudes and post-fault instability of units. A multi-state model is established to provide an optimal resilience enhancement strategy for the power system considering the uncertainty of weather forecasts and cost-effectiveness. The main contributions of this paper are:

1) A fragile model is developed to evaluate the nodal SCF probability with subject to an extreme weather event, which divides the short-circuit rate into the aging-based reference value and the covariant part determined by the severity of atmosphere weather.
2) An integrated extreme weather response framework for transmission systems is proposed, which utilizes an MINLP model to provide optimal line switch shifting, generation rescheduling, and load shedding schemes to ensure the system resilience against cascading impacts of triggered SCFs.
3) Considering the uncertain forecasts from NAS, a multi-state model is established to search for the most cost-effective grid resilience enhancement scheme, in which the expected urgent adaptions of the initial scheme subject to weather state transition are included in the overall cost.

II. Fragile Model

In this section, a fragile model is introduced to map from weather parameters to SCF rates of overhead lines, which is illustrated with a hurricane case. The fragile model is divided into three steps, aging-based reference SCF rate modeling, weather-induced covariant SCF rate calculation, and overall SCF rate calculation.

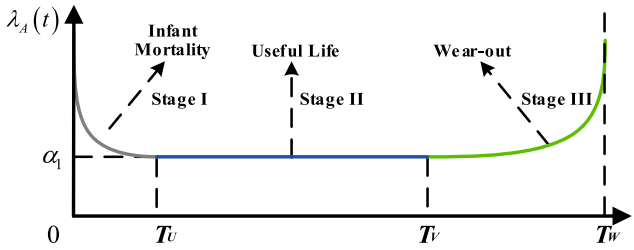

Fig. 1. Bathtub curve for reference SCF rate.

A. Aging-Based Reference SCF Rate Modeling

The reference SCF rate without consideration of extreme external conditions is mainly determined by insulation material damage caused by various defects, aging or accidental factors [19], which can be well described with the Bathtub curve.

As shown in Fig. 1, the reference SCF rate generally passes through three stages, including the infant mortality, useful life, and wear out. Specifically, the SCF in Stage I is relatively frequent which is caused by defects in design, materials and production process, or improper use. The SCF in stage II is caused by some random factors whose occurrence rates are relatively constant. Stage III is associated with the aging of insulation materials, where the SCF rate grows rapidly with the increasing accumulated service time. Note that long-term strict test and quality inspection will be carried out before the electrical equipment is deployed, the infant mortality stage is usually skipped or compressed to a very short duration. In this paper, stages II and III are considered. Weibull distribution, as the most deployed mathematical model to describe the Bathtub curve [20], was used for the reference SCF rate modeling.

$$\lambda_A(t) = \begin{cases} \alpha_1 & ; \quad T_U \le t < T_V \\ \alpha_2 \mathrm{e}^{\beta_2 t} & ; \quad T_V \le t < T_W \end{cases} \tag{1}$$

The parameters in Eq. (1) can be fitted through long-term statistics of a large number of samples or obtained through modeling the physical aging mechanism of materials.

B. Covariant SCF Rate Modeling Under the Extreme Weather

Considering the extreme weather, the described SCF rates in Fig. 1 are greatly magnified. Under a hurricane, most SCFs are caused by the falling towers or trees, thus the SCF rate of overhead lines is mainly influenced by wind direction and speed. The wind load function L_W for a transmission line with coordinates (x, y) can be expressed as follows [21]:

$$L_W(x,y,t) = \varpi(t)\left[\varepsilon_1 \exp\left(-\frac{R^2}{2\gamma_1^2}\right) - \varepsilon_2 \exp\left(-\frac{R^2}{2\gamma_2^2}\right)\right] \tag{2}$$

$$R = \sqrt{[(x-\kappa_x(t)]^2 + [y-\kappa_y(t)]^2} \tag{3}$$

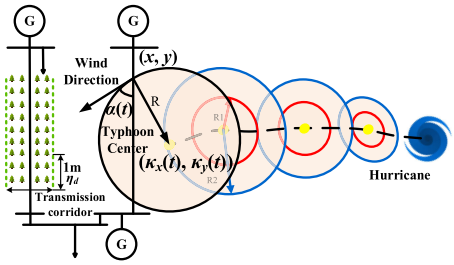

Fig. 2. A moving hurricane influencing a transmission line.

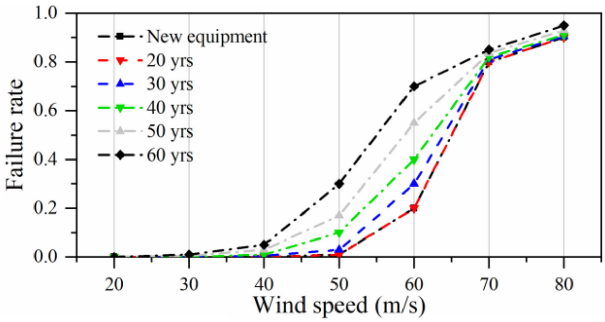

Fig. 3. Fragility curves of overhead lines at different years.

where ε_1 and ε_2 are hurricane intensity parameters; γ_1 and γ_2 denote influence scopes; R is the distance between hurricane center and transmission line; (x, y) and $(\kappa_x(t), \kappa_y(t))$ are coordinates of the line and the wind center, respectively. $\varpi(t)$ denotes the influence factor of wind direction on wind load, which is defined as follows:

$$\varpi\left(t\right) = \sin\alpha\left(t\right) \tag{4}$$

$\alpha(t)$ is the angle by which the wind hits the line, which is shown in Fig. 2.

The relationship between wind load and covariant SCF rate of the transmission line can be described below:

$$\lambda_W(t) = \exp\left[a_1 \frac{L_W\left(x, y, t\right)}{V_d} + a_2\right] \frac{\eta_d \eta_h}{H} L \tag{5}$$

where a_1 and a_2 are parameters obtained from historical statistics; V_d is the design wind speed of transmission line; η_d and η_h are the vegetation density (1/m) and average height (m) within the specified 35m wide transmission corridor; H and L are the height (m) and length (km) of the transmission line.

C. Overall SCF Rate Calculation

As the SCF rate has not yet been well studied quantitatively in the prior-art studies, the modeling of the overall SCF rate considering covariates is still blurring. This paper acquires some realistic operation and SCF data from East China Power Grid to illustrate the relationship among SCF rate, equipment aging degree, and extreme weather conditions, which is shown in Fig. 3. The trend of SCF rate is consistent with that in [22].

As shown in Fig. 3, the SCF rate of new equipment is basically the same as that of 20-year-old equipment under different wind speeds. In other words, when the aging of equipment is not so serious, the influence of aging on the SCF rate under certain extreme weather events can be ignored. Then, the weather parameters play a leading role in causing SCFs. However, if the aging reaches a certain threshold, its amplification effect on the SCF rate under the extreme weather events gradually appears. Moreover, at a certain aging degree, the varying trend of SCF rate is close to that of covariant SCF rate modeled with Eq.(5) in shape, which is approximately *S*-type. This shows that aging plays a role of scaling and does not fundamentally change the trend of failure rate with subject to wind speed. Thus, the following linear function is used to express the overall SCF rate under the combined effect of aging and extreme weather factors:

$$\lambda\left(t\right) = \lambda_W\left(t\right) \psi_1\left[\lambda_A\left(t\right), \lambda_0\right] \tag{6}$$

$$\psi_1\left[\lambda_A\left(t\right), \lambda_0\right] = \begin{cases} \lambda_A\left(t\right)/\lambda_0, & \lambda_A\left(t\right) > \lambda_0 \\ 1, & \lambda_A\left(t\right) \le \lambda_0 \end{cases} \tag{7}$$

where ψ_1 represents the penalty operator for reference SCF rate $\lambda_A(t)$ exceeding a given failure rate λ_0.

In order to evaluate the SCF rate more accurately, both extreme weather and equipment aging require additional data collection efforts [23]. Subsequently, with the accumulation of short-circuit fault records, equipment aging and extreme weather data acquisition, some parameter estimation or machine learning methods can be used to specify the parameters of SCF rate calculation.

The SCF probability of line l in $[0, t_m]$ can be obtained via the integral of corresponding instantaneous rates [21]:

$$\rho_l = 1 - \exp\left[-\int_0^{t_m} \lambda\left(t\right) dt\right] \tag{8}$$

Finally, SCFs whose occurring probabilities are greater than a given threshold ρ_{thre} are considered to be credible and included in the set of expected faults. The value of this threshold is an important input of the proposed model, which reflects the risk preference of system operators. The detailed model to select the given threshold ρ_{thre} is given in Section IV-B.

III. Extreme Weather Event Response Schema

In this section, the evolution or spreading of a SCF in a transmission system is investigated, including the relay protection and system stability control stages, to conduct the contingency management strategy pertinently.

Specifically, the circuit breaker is utilized in the relay protection stage to remove the fault. Generally, the transmission line fault can cause huge SCCs, which cannot be cut through circuit breakers when the current exceeds the limited value. Restraining SCC within the limit is the first task of extreme weather event management. Besides, SCF is considered to be a severe disturbance for the power system operation, which might cause transient instability. Thus, post-fault transient stability maintenance is another task of SCF management.

The response framework of a transmission system for extreme weather events is shown in Fig. 4. The activities deployed by grid operators include non-networked schemes without adding equipment and networked ones associated with grid planning.

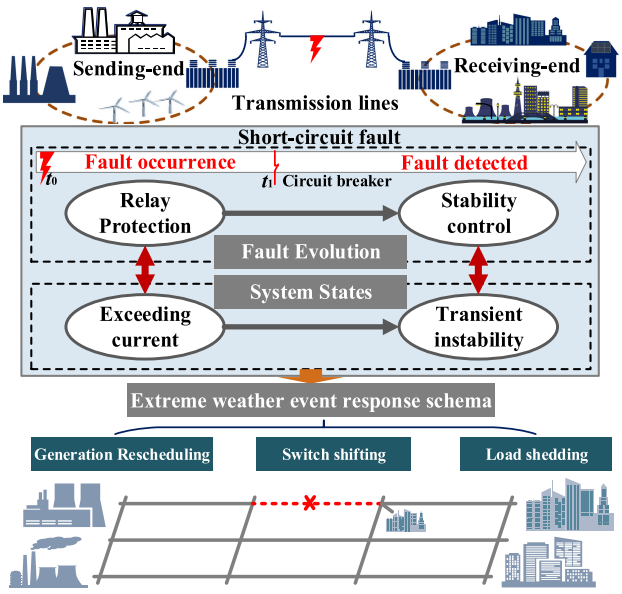

Fig. 4. Response framework for extreme weather events.

As for the out-of-rage SCC limitation, the deployment of FCLs is a kind of networked scheme, while the switch shifting and bus splitting belong to non-networked schemes. As the NAS is in the short-term temporal scale, which is mainly performed one or two weeks ahead. Networked schemes cannot be installed so timely. Therefore, non-network measures like switch shifting are utilized to limit the SCC in the proposed schema. For transient stability concerns which are in operation scale, non-networked schemes such as generation rescheduling and load shedding are deployed.

The aforementioned non-networked strategies against SCFs caused by extreme weather events are modeled as follows.

A. Short-Circuit Current Limiting

As mentioned before, the line switch shifting is utilized to limit the exceeding SCCs. The detailed scheme cost and the current limiting effect are described as follows:

1) Cost of Line Switch Shifting: Switch shifting on lines may result in direct load loss and the change of system operating conditions. The overall switch shifting scheme cost C_1 is formulated as follows:

$$C_1 = \sum_{(i,j)\in\Omega_B} \chi_{ij} c_{ij} \tag{9}$$

where χ_{ij} represents the switch shifting status on line *i-j*. Ω_B is the set of switches to be shifted. c_{ij} is the cost of switch shifting on line *i-j*, which include the direct load loss cost, and the difference of system operation cost (F_B-F_A). F_B and F_A are determined with the optimal power flow model before and after deploying the switch shifting scheme.

2) The Current Limiting With Switch Shifting: Generally, the SCCs of three-phase faults are higher than single-phase ones [11]. Here, the effect of switch shifting on SCC limiting is illustrated with a three-phase SCF. The three-phase SCC [24] should be limited to the given threshold I_M:

$$I_b = \frac{{V_b}^0}{X_{bb}} \le I_M \tag{10}$$

where ${V_b}^0$ and X_{bb} are the pre-fault voltage and the self-impedance of bus *b*.

An effective method for SCC limiting is to modify the node admittance matrix and thus increase the self-impedance of the corresponding buses [11]. If the impedance of line *l* is added by Δx_l, the incremental of the diagonal element X_{bb} is [25]:

$$\Delta X_{bb} = -\frac{(X_{bi} - kX_{bj})^2}{-({x_{l0}}^2 + \Delta x_l x_{l0})/\Delta x_l + X_{ii} + k^2 X_{jj} - k(X_{ij} + X_{ji})} \tag{11}$$

where $X_{bi}, X_{bj}, X_{ii}, X_{jj}, X_{ij}$ and X_{ji} are all elements of impedance matrix *X*; *k* is the standard voltage ratio imputed to *i* side; x_{l0} is the initial impedance of line *l* from bus *i* to *j*. The switch shifting on line *l* is equivalent to $\Delta x_l \to \infty$, whose effect is:

$$\Delta X_{bb} = -\frac{(X_{bi} - kX_{bj})^2}{-x_{l0} + X_{ii} + k^2 X_{jj} - k(X_{ij} + X_{ji})} \tag{12}$$

3) Islanding Detection: The switch shifting on lines may cause islanding, which should be excluded from the feasible solutions. An islanding detection technique based on the incidence matrix [26] is introduced to screen the candidate switches to be shifted. The bus-branch incidence matrix can be expressed as an $N_b \times N_l$ matrix $\boldsymbol{A} = (a_{i,l})_{Nb\times Nl}$ through the bus set Ω_b, the line set Ω_l, and the line status Ω_s. The detailed elements of $\boldsymbol{A}$ are:

$$a_{il} = \begin{cases} 1 & i \subset l \\ 0 & i \not\subset l \end{cases} \tag{13}$$

where $i = 1, 2, \ldots N_b$, $l = 1, 2, \ldots N_l$, and $i \subset l$ represents that bus *i* is connected to line *l*, otherwise $i \not\subset l$. When the switch on line *l* breaks, the elements of column *l* in $\boldsymbol{A}$ are all set to 0.

Then the first level bus-bus incidence matrix can be expressed as $C^{(1)} = ({c^{(1)}}_{i,j})_{Nb\times Nb}$, in which the elements are:

$$c_{ij}^{(1)} = \bigcup_{k=1}^{N_l} (a_{ik} \cap a_{jk}) \tag{14}$$

Moreover, the final level bus-bus incidence matrix $C^{(NI)}$ is calculated based on $C^{(1)}$:

$$C^{(N_l)} = \prod_{l=1}^{2^{(N_l-1)}} C^{(1)} \tag{15}$$

If the final level bus-bus incidence matrix $C^{(NI)}$ contains 0 elements, the initial switch shifting scheme can cause islanding and should be removed.

B. Transient Stability Maintaining

The generation rescheduling and load shedding are adopted for transient stability maintenance. The corresponding cost and constraints are described as follows:

1) Transient Stability Cost: The total operating costs of power system considering the generation rescheduling and load shedding are as follows:

$$C_o = \sum_{i\in N_G}\sum_{g\in NG_i} C_{ig}^{P}\left(P_{ig}\right) + \sum_{i\in N_L}\sum_{s\in NL_i} L_{pis} D_s\left(d_o\right) \quad (16)$$

where P_{ig} and $C_{ig}{}^{P}$ are the active power output and the generation cost function of generator g on bus i; L_{pis} represents the load curtailment of user s on bus i; N_G and N_L are the set of generator buses and load buses; NG_i and NL_i are the set of generators and loads on bus i; d_o represents the outage time, $D_s(d_o)$ is the cost damage function.

2) Steady Constraints and Dynamic Equations: First, the power flow equations are given as follows:

$$\begin{aligned}
&\sum_{g\in NG_i} P_{ig} - \sum_{s\in NL_i}\left(P_{is} - L_{pis}\right) \\
&\quad = \sum_{j=1}^{N_b} V_i V_j \left(G_{ij}\cos\theta_{ij} + B_{ij}\sin\theta_{ij}\right) \\
&\sum_{g\in NG_i} Q_{ig} - \sum_{s\in NL_i}\left(Q_{is} - L_{qis}\right) \\
&\quad = \sum_{j=1}^{N_b} V_i V_j \left(G_{ij}\sin\theta_{ij} - B_{ij}\cos\theta_{ij}\right)
\end{aligned} \quad (17)$$

where N_b is the number of buses; P_{is} and Q_{is} is the active and reactive load of user s on bus i; Q_{ig} is the reactive power of generator g on bus i; V_i and θ_i are the voltage magnitude and angle of bus i; G_{ij} and B_{ij} are the admittance of line i-j. Besides, the limits of the generator outputs and nodal voltages are also considered in the TSCOPF.

Then, a classical generator model in [27] is adopted:

$$E_g\angle\delta_g^0 = \dot{V}_i + \frac{j\left(P_{ig} - jQ_{ig}\right)}{\overset{*}{V}_i} X'_{dg} \quad (18)$$

where E_g, $\delta_g{}^0$ and X'_{dg} represent the internal voltage magnitude, initial rotor angle and direct-axis transient reactance of generator g. The initial value equation is transformed into the following real and imaginary parts:

$$\begin{cases} E_g V_i \cos\left(\delta_g^0 - \theta_i\right) - V_i^2 - Q_{ig} X'_{dg} = 0 \\ E_g V_i \sin\left(\delta_g^0 - \theta_i\right) - P_{ig} X'_{dg} = 0 \end{cases} \quad (19)$$

Finally, two groups of discretized swing equations are given to describe the dynamics:

$$\begin{aligned}
&\delta_g^t = \delta_g^{t-1} + \frac{\Delta t}{2}\left(\omega_g^t + \omega_g^{t-1} - 2\right)\omega_N \\
&\omega_g^t = \omega_g^{t-1} \\
&\quad + \left[\Delta t\left(2P_{ig} - D_g\omega_g^t - D_g\omega_g^{t-1} - P_{eg}^t - P_{eg}^{t-1}\right)\omega_N\right]/(2M_g)
\end{aligned} \quad (20)$$

where ω_N is the synchronous rotor speed; Δt is the step length; $\delta_g{}^t$ and $\omega_g{}^t$ are rotor angle and rotor speed of generator g at time step t; M_g and D_g are the inertial constant and damping constant of generator g. $P_{eg}{}^t$ is the active electromagnetic power of generator g at time step t, which is given by:

$$P_{eg} = E_g \sum_{n=1}^{NG} E_n\left[G_{gn}\cos\left(\delta_g - \delta_n\right) + B_{gn}\sin\left(\delta_g - \delta_n\right)\right] \quad (21)$$

where NG is the number of generators; G_{gn} and B_{gn} represent the reduced admittance between generator g and n. Transient stability constraints are as follows:

$$-\delta_{\max} \le \delta_g^t - \delta_{COI}^t = \delta_g^t - \frac{\sum_{g\in NG}\delta_g^t M_g}{\sum_{g\in NG} M_g} \le \delta_{\max} \quad (22)$$

where $\delta_{COI}{}^t$ is the center of inertia (COI) at time t and $\delta_{\max}$ represents the angle deviation thresholds with respect to the center of inertia.

C. Formulation of the MINLP in the Proposed Schema

Based on the previous SCC limitation and stability maintenance models, the optimal integrated response strategy of a transmission system against an extreme weather event of interest can be obtained by solving the following combined MINLP. The objective function is to minimize the overall costs of switch shifting, generation rescheduling, and load shedding.

$$\begin{aligned}
\min &\sum_{(i,j)\in\Omega_B} \chi_{ij} c_{ij} + \sum_{i\in N_G}\sum_{g\in NG_i} C_{ig}^{P}\left(P_{ig}\right) \\
&+ \sum_{i\in N_L}\sum_{s\in NL_i} C_{is}^{L}\left(L_{pis}\right)
\end{aligned} \quad (23)$$

Subject to the following constraints:
SCC limitation constraints:

$$\forall I_b \le I_M \quad (24)$$

Transient stability constraints:

$$-\delta_{\max} \le \delta_g^t - \delta_{COI}^t \le \delta_{\max} \quad (25)$$

Other operational and dynamic security constraints: (10)–(15), (17)–(22)

The decision variables include 0–1 variable of switch shifting status χ_{ij}, continuous variables of nodal load curtailment L_{pis} and generator active power output P_{ig}. χ_{ij} indicates the status of the switch. $\chi_{ij} = 1$ means that the switch on line i-j is opened and $\chi_{ij} = 0$ means it is closed. Constraint (24) denotes that nodal SCCs should not exceed the threshold I_M. Constraint (25) means the generator rotor angle oscillation should be limited within a range at each time step. Note that both the objective function and SCC constraint contain 0-1 variables χ_{ij}. Thus, the proposed MINLP is nonconvex.

IV. Multi-State Modelling of Transmission System Resilience Enhancement

The weather forecast is of complexity. As illustrated in Fig. 5, for a newly generated extreme hurricane, usually several possible moving paths [28], and intensities [29] will be announced by the meteorological bureaus or groups but not a deterministic one [30]. Consequently, power systems are faced with great

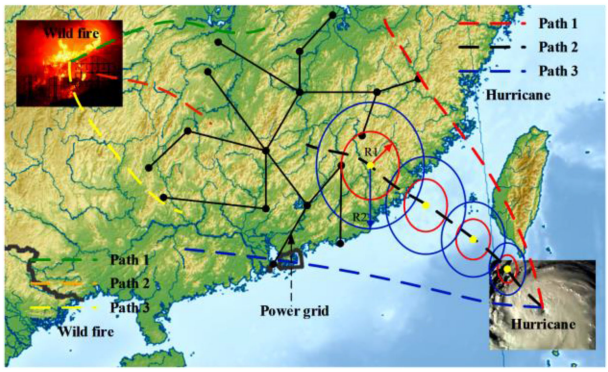

Fig. 5. Uncertain moving paths of extreme weather events.

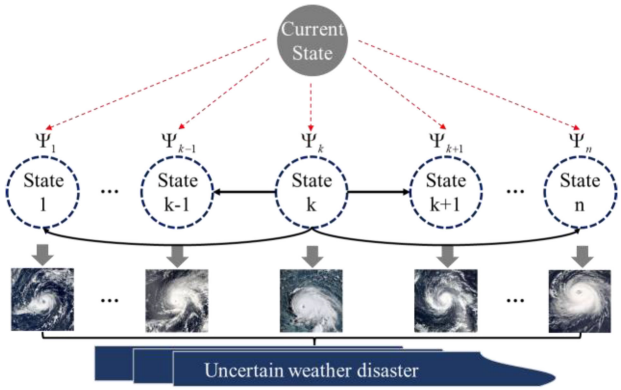

Fig. 6. Multi-state resilience enhancement model against short-circuits.

uncertainties in pre-event dispatching. In this section, a comprehensive multi-state model is established to describe the uncertain influences of extreme weather events on the power system in terms of triggered SCFs. Then a two-stage decision approach is proposed to achieve a balance between economy and system resilience.

A. Multi-State Resilience Enhancement Against SCFs

In the established model, states represent certain sets of SCFs due to different predicted hurricane situations. Each state corresponds to a specific initial defending strategy and their performance can be described in terms of the following initial defending strategy cost and state probability:

$$\mathbb{C}_k = f_k\left(\mathbf{\Omega}_k^{\mathrm{T}}, \mathbf{\Omega}_k^{\mathrm{S}}\right) = C_k^1 + C_k^2 \tag{26}$$

$$P_k = \tilde{p}_s \prod_{l \in S_k} \rho_l \prod_{o \notin S_k} (1 - \rho_o) \tag{27}$$

where $\mathbb{C}_k$ and P_k represent the prevention cost of state k and its corresponding probability; ${\Omega_k}^T$ and ${\Omega_k}^S$ represent the generation rescheduling/load shedding, and switch shifting strategies; ${C_k}^1$ and ${C_k}^2$ are the costs of system transient stability maintenance and SCC limitation, respectively; $\tilde{p}_s$ is the standardized probability of the s-th hurricane, which is obtained based on hurricane forecast; S_k is the set of the short-circuit lines in state k under the s-th hurricane scenario, ρ_l is SCF probability of line l obtained with the fragile model.

Specially, Eq. (26) represents the initial prevention cost of state k, which is a function of the generation rescheduling/load shedding ${\Omega_k}^T$, and switch shifting strategies ${\Omega_k}^S$. These optimal integrated response strategy of a transmission system against an extreme weather event of interest can be obtained by solving the proposed MINLP in Section III-C. Besides, the prevention cost can also be represented as the summation of the costs of system transient stability maintaining ${C_k}^1$ and SCC limiting ${C_k}^2$. With regard to Eq. (27), it represents the probability of state k, which is obtained by multiplying the standardized probability $\tilde{p}_s$ of the s-th weather scenario and the calculated SCF or normal operation event probabilities given by the fragile model in the corresponding scenario. For instance, there is a set of short-circuit lines in state k, the probability of the expected fault in the s-th weather scenario is the product of the SCF probabilities of the short-circuit lines and the normal operation probabilities of the non-fault lines.

System state transition may occur due to errors in NAS result of the extreme weather event. In other words, when the hurricane lands, the situation may not be the same as previously expected. Consequently, an urgent adaption of the initial defending strategy is required. The transition probability is a conditional probability associated with both the current and future states. If the correlation of states is ignored, then the transition formula from state k to h can be expressed as:

$$\mathbb{C}_{k\to h} = f_{k\to h}\left(\mathbf{\Omega}_{k\to h}^T, \mathbf{\Omega}_{k\to h}^S\right) = C_{k\to h}^1 + C_{k\to h}^2 \tag{28}$$

$$P_{k\to h} = P_h = \tilde{p}_m \prod_{l \in S_h} \rho_l \prod_{o \notin S_h} (1 - \rho_o) \tag{29}$$

where $\mathbb{C}_{k\to h}$ represents the adaption cost of state k to h; $P_{k\to h}$ represents the transition probability from state k to h; $C_{k\to h}^1$ and $C_{k\to h}^2$ denote the system stability maintenance and SCC limitation costs from state k to h, separately; $\Omega_{k\to h}^T$ and $\Omega_{k\to h}^S$ represent the generation rescheduling/load shedding and switch shifting strategies from state k to h. $\tilde{p}_m$ is the standardized probability of the m-th hurricane; S_h is the set of the short-circuit lines in state h under the m-th hurricane scenario. Due to the higher requirement of response speed, the cost parameters of urgent adaption are higher than those of the initial defending, such as the climbing cost of units and shedding cost of loads.

The urgent adaption in the second stage is to expand the initial defending strategy to an updating state. As shown in Fig. 6, considering the probabilistic state transition, the overall cost of resilience enhancement strategy under state k can be modelled as the sum of the initial defending cost and the expected urgent adaption cost of the initial plan being adapted to other future states, which is expressed as follows:

$$\min_{k \in S^{pre}} E_k = \mathbb{C}_k + \sum_{h \in S^{pre}, h \neq k} \mathbb{C}_{k\to h} P_{k\to h} \tag{30}$$

where S^{pre} represents the set of expected faults.

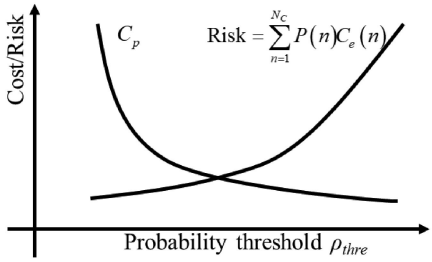

Fig. 7. Relationship between the control cost/system risk and ρ_{thre}.

B. State Generating Model

As introduced above, the probability threshold ρ_{thre} is mainly determined in consideration of the risk preference of system operators. Specifically, the smaller the threshold is set, the more SCFs are considered in the fault defending process, compromising the economy of system operation while benefiting the security. The appropriate probability threshold can be determined by coordinate the fault defending cost and system risk. For one state, the optimization model to obtain the probability threshold is given:

$$\min_{\rho_{thre}} C_T = C_p + \lambda_R \sum_{n=1}^{N_C} P(n) C_e(n) \tag{31}$$

where λ_R is the risk reference coefficient. C_p is the total cost of defending against all the expected SCFs whose probabilities are larger than ρ_{thre}. *Nc* is the number of unexpected SCFs whose probabilities are smaller than ρ_{thre}. $C_e(n)$ is the severity of the power system when the *n-th* unexpected SCF happens. $C_e(n)$ can be measured by the cost of urgent generation rescheduling and load shedding. $P(n)$ represents the probability of the *n-th* unexpected SCF. C_p and $C_e(n)$ can be obtained by solving Eq. (26), Eq. (28), respectively.

It should be noted that C_p has some monotone decreasing relationship with ρ_{thre}, as is illustrated in Fig. 7. Since the feasible region of the expected fault defending optimization problem will definitely enlarge as ρ_{thre} increases. Moreover, the system risk has some monotone increasing relationship with ρ_{thre}. When ρ_{thre} is very small or large, the value of C_T will be large. Thus, C_T has a minimum value, which is mainly determined by ρ_{thre} under the given risk coordination coefficient [31]. After ρ_{thre} is determined, the state of the system is determined accordingly.

C. Traversal Procedure

As illustrated in Fig. 8, the process of the multi-state modeling for the transmission system resilience enhancement can be divided into four steps:

Step 1. State generating: Based on released forecasts of extreme weather events, the SCF rates of transmission lines are calculated with the fragile model in Section II. The faults whose probabilities are greater than ρ_{thre} are added to the expected fault set. Lines with higher fault rates and their combinations are utilized to generate system states as well as the assessed probabilities.

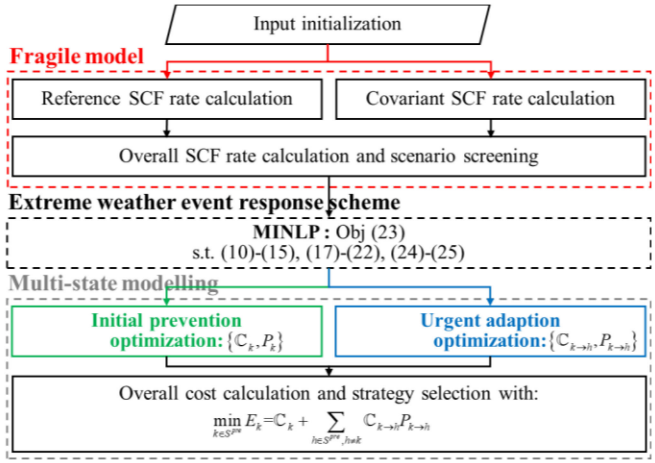

Fig. 8. The flowchart of the multi-state modeling for resilience enhancement.

Step 2. Initial prevention: According to the obtained states, the initial prevention strategy and its cost are determined by solving the MINLP defending model. Shifted switches are selected to limit SCCs and load curtailment as well as generation adjustments are optimized to guarantee the transient stability under each initial system state.

Step 3. Urgent adaption: All possible state transitions from initial states to others are evaluated. The urgent adaption strategies are obtained by solving the MINLP defending model to handle possible abrupt weather changes.

Step 4. Strategy selection: The initial prevention cost and expected urgent adaption cost are summed for each state. The initial preventive measure with the lowest overall cost is selected as the final scheme to enhance the resilience of the power system before the arrival of the extreme weather event.

V. Solution Method

As mentioned above, the proposed MINLP is non-convex and high dimensional. To solve the problem, we reformulated the proposed MINLP model. Then, a searching space reduction technique and a combined heuristics and CNDIPM solution method are developed in this section.

A. Problem Reformulation

In regard to the proposed problem, conducting the switch shifting strategy is not necessarily capable to guarantee that the out-of-range SCCs can be limited below the threshold. The load shedding and generation rescheduling cannot definitely guarantee the transient stability of the post-fault system. Moreover, the conducted solutions may be contradictory in terms of the effects of stability maintaining and current limiting. Thus, there may be no solution to this MINLP.

In this paper, a reformulation strategy is adopted to deal with this problem. Specifically, a penalty function for the critical constraints [32] is introduced, and the original constrained problem

is transformed into the following form:

$$\min\left\{\left(\sum_{(i,j)\in\Omega_B}\chi_{ij}c_{ij}+\sum_{i\in N_G}\sum_{g\in NG_i}C_{ig}^{P}\left(P_{ig}\right)+\sum_{i\in N_L}\sum_{s\in NL_i}C_{is}^{L}\left(L_{pis}\right)\right)+\sum_{b=1}^{Nb}\left(\psi_o\left(I_b,I_M\right)\lambda_c\right)+\sum_{g=1}^{NG}\sum_{t=1}^{T_s/\Delta t}\left(\psi_o\left(\left|\delta_g^t-\delta_{COI}^t\right|,\delta_{\max}\right)\lambda_s\right)\right\} \tag{32}$$

Subject to the following operational constraints: (10)–(15), (17)–(22)

The penalty operator ψ_o is formulated as follows:

$$\psi_o\left(m_1,m_2\right)=\begin{cases}m_1-m_2, & m_1>m_2,\\ 0 & m_1\le m_2.\end{cases} \tag{33}$$

In (32), the first part denotes the original objective function, while the second and the third parts denote the penalties of the exceeding fault currents and the transient instability, respectively. It should be noted that the penalty coefficients λ_c and λ_s are set to very large numbers (such as 10e6) to ensure no violation of the solutions in terms of fault current limitation and post-fault transient power angle convergence in most cases (these two penalty items are zero).

B. Searching Space Reduction

In the proposed problem, the discrete and continuous variables are coupled, which increases the difficulty of optimization. Therefore, we try to divide it into discrete and continuous sub-problems and deal with them separately and interactively. For the discrete or current limiting sub-problem, it will be very time-consuming to restart the searching of switch shifting schemes without any prior knowledge for each iteration. Considering the generality of switch shifting schemes, a sensitivity-based searching space reduction technique [33] is introduced to choose some switching candidates or line switching patterns so as to avoid the curse of dimensionality and speed up the solution. Considering the excessive level of SCCs and impedance incremental sensitivity factor of all buses, the comprehensive sensitivity of the switch shifting on line l to the whole system is expressed as follows:

$$\xi_s\left(l\right)=\sum_{b\in N_I}\left[\left(\frac{I_b}{I_{thre}}\right)^{\tau}\frac{-\left(X_{bi}-kX_{bj}\right)^2}{X_{ii}+k^2X_{jj}-2kX_{ij}-x_{l0}}\right] \tag{34}$$

where τ is an adjustment coefficient; N_I is the set of the buses whose fault currents exceed the threshold. $\xi_s(l)$ is used to choose the candidate shifted switches to limit SCCs.

C. Heuristics Solution

For the continuous or stability control sub-problem, as a widely-used analytic tool, the TSCOPF solver is utilized to calculate the stability-oriented scheme considering the fact that power systems are transient stability in most cases.

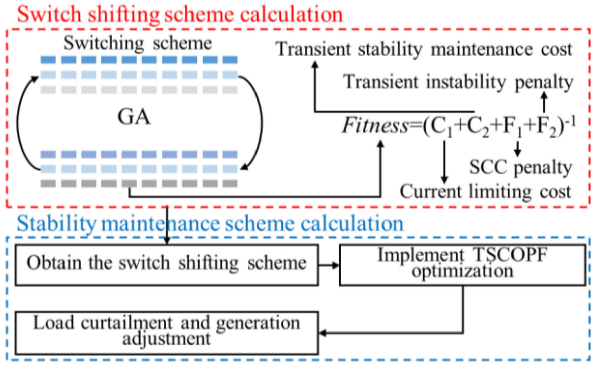

Fig. 9. The procedure of the proposed solution method.

Based on the above content, an efficient heuristic based on GA and CNDIPM is developed to solve the nonconvex reformulated problem considering an interaction strategy, which is illustrated in Fig. 9. The framework of the method can be decomposed into two levels, the top level is the decision sub-problem of switch shifting, the bottom level is the sub-problem of TSCOPF optimization. Firstly, within the candidate shifted switches indicated by $\xi_s(l)$, GA is utilized at the top level to generate a parent population, in which each chromosome denotes a raw configuration scheme of switch shifting. For each chromosome, its cost of switch shifting C_1 is calculated, and then the two following calculations are performed:

1) The nodal SCCs are calculated and the corresponding current penalty F_1 is quantified.
2) The CNDIPM [14] is utilized at the bottom level to obtain the optimal load curtailments and generation adjustments. The corresponding cost is denoted as C_2 and the transient stability instability penalty F_2 is evaluated.

For each switch shifting scheme, its fitness is defined as the reciprocal of the summation of the current limiting cost C_1, the SCC penalty F_1, the transient stability maintenance cost C_2, and the transient stability instability penalty F_2, which is written as $Fitness=(C_1+F_1+C_2+F_2)^{-1}$.

Indicated by the obtained fitness values, elite switch shifting schemes are selected with higher fitness values. Then, crossover and mutation are performed to generate an offspring population and the iterative evolution continues until the maximum iteration is reached. The shifting scheme with the highest fitness in the last population is selected as the final suggested scheme, as well as its corresponding load shedding and generation rescheduling solution. It should be noted that the cases with unsolvable TSCOPF can be ignored as the nonzero penalty term restricts the fitness of the corresponding solutions.

VI. Case Study

The New England 39-bus system is adopted to verify the proposed method. The simulation time is 1s with a step of 0.05s. All the SCFs are uniformly set to be three-phase-to-ground ones occurring at 0 s and cleared by tripping the fault lines at 0.1s. The parameters of hurricane and lines are listed in Table I.

TABLE I
THE PARAMETERS OF HURRICANE AND TRANSMISSION LINES

Parameters	Values	Parameters	Values
ε_1(G1)	50 m/s	ε_2(G1)	20 m/s
ε_1(G2)	45 m/s	ε_2(G1)	18 m/s
γ_1	120 km	γ_2	15km
V_d	30 m/s	Δt	0.05s
a_1	11	a_2	-8

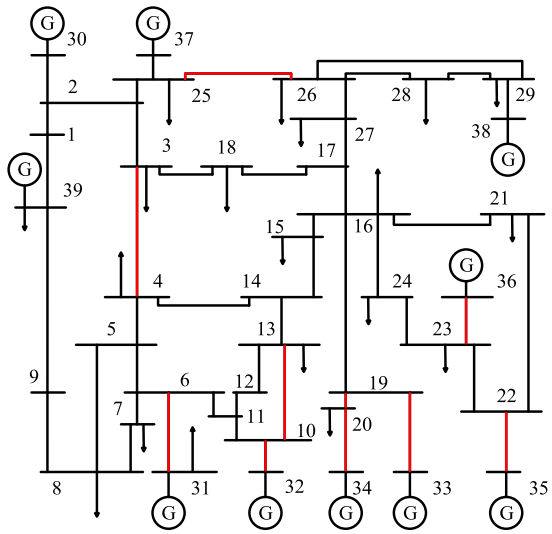

Fig. 10. Topology diagram of the New England system.

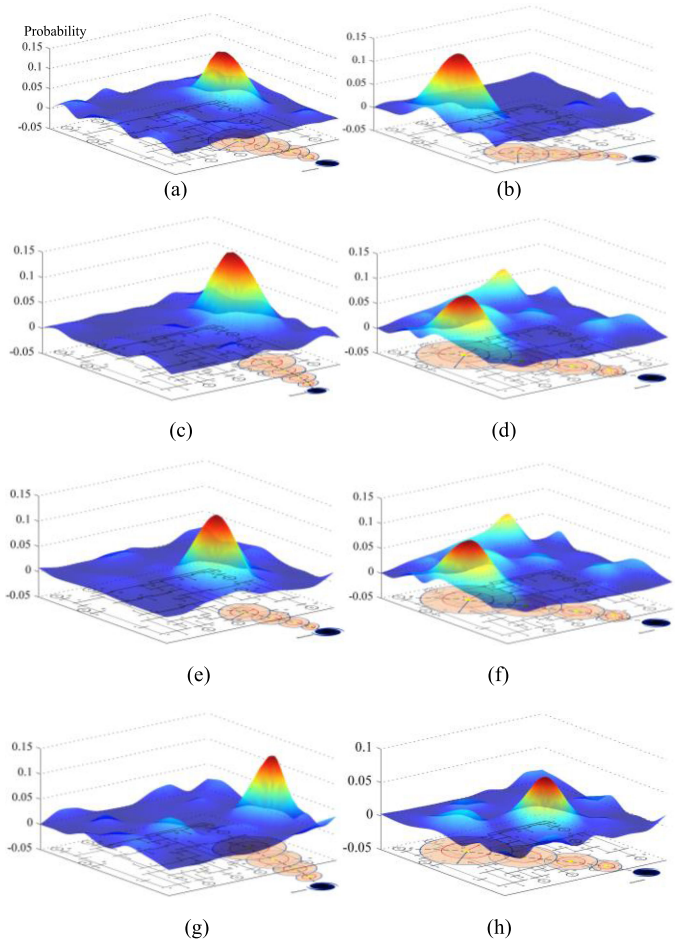

Fig. 11. Failure rates of transmission lines under different hurricanes. (a) Path 1: Grade 1. (b) Path 2: Grade 1. (c) Path 3: Grade 1. (d) Path 4: Grade 1. (e) Path 1: Grade 2. (f) Path 2: Grade 2. (g) Path 3: Grade 2. (h) Path 4: Grade 2.

The topology diagram of the system is shown in Fig. 10. Moreover, there are two aging conditions of lines considered. Note that the red lines in Fig. 10 are assumed to be in the wear-out stage of the bathtub curve, while the other transmission lines are at the stage of useful life. Specifically, line 25–26, 3–4, 6–31, 10–13, 10–32, 20–34, 19–33, 22–35, and 23–36 are in stage III, and their failure rate is 0.06 (1/year). The failure rate of the other lines (In stage II) is 0.008 (1/year).

A. Scenario Generating

In this paper, both the moving path and hurricane strength are considered to generate the SCF scenarios. Referring to a historical Pacific Ocean hurricane available from the China hurricane weather website [34], four possible landings or moving paths and two possible strengths are revealed to the public. Thus, eight hurricane scenarios are considered to guide power system resilience enhancement. The detailed short-circuit probabilities of lines subject to hurricane forecasts are determined by the fragile model, which are shown in Fig. 11.

The expected SCF event's probabilities are determined with the standardized probabilities of hurricanes and the corresponding theoretical SCF probabilities of transmission lines. According to the risk preference of the system operator, the number of considered expected faults is determined. Then, the expected SCF states are selected in the order of ultimate probability from high to low. The probability threshold for a SCF event to be integrated into the expected SCF set is set to be 0.1 according to the risk preference of system operators. Here, 8 SCF states comply with this threshold, and the corresponding expected faults are shown in Table II. Note that the probability of the second-order SCF denoted as a product of isolated failure rates is much lower than that of the first-order SCF. Thus, the case of simultaneous faults is ignored and there is one line encountering SCF for each state.

TABLE II
THE PROBABILITY OF DIFFERENT SCENARIOS

Scenarios	lines	probability	Scenarios	lines	probability
1	19-20	0.1651	5	20-34	0.1247
2	6-31	0.1529	6	22-35	0.1478
3	10-13	0.1013	7	23-36	0.1454
4	19-33	0.1306	8	25-37	0.1124

B. Sensitivity Analysis

The sensitivity factors of transmission lines are shown in Fig. 12. The top 10 transmission lines with the largest comprehensive sensitivity factors are line 16–17, 2–30, 17–27, 16–27, 28–29, 26–28, 26–29, 15–16, 22–23 and 14–15. Some switch shifting options like the switches on line 22–35 and line 25–37

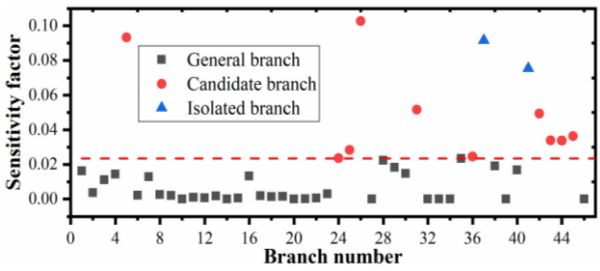

Fig. 12. Candidate branches with the largest sensitivity factors.

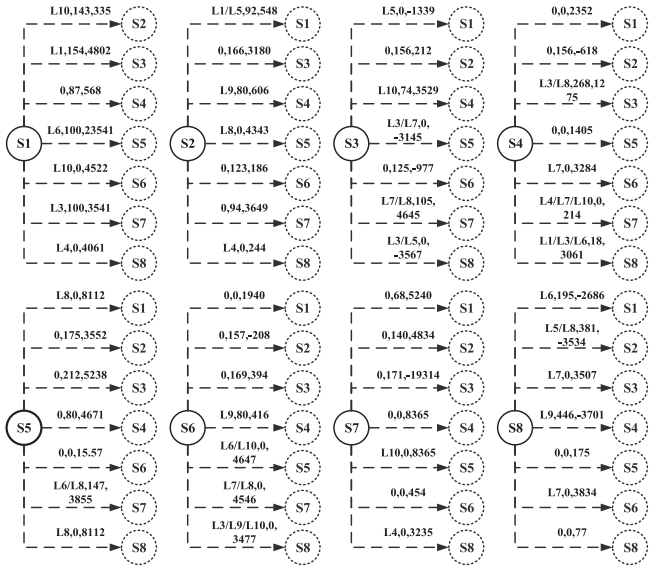

Fig. 13. Urgent adaption strategies of 8 states.

TABLE III
THE INITIAL PREVENTION STRATEGIES

Scenario	Strategies	Scenario	Strategies
1	L5, 160MW, 1381$	5	L3/L7, 0, 3189$
2	L6, 157MW, 1273$	6	124MW, 1445$
3	163MW, 5796$	7	L6/L10, 0, 3208$
4	L9, 81MW, 1862$	8	L4, 0, 1539$

are excluded, which caused islanding with Eq. (15). The optimal switch shifting scheme is searched among the above 10 candidate lines.

C. Suggested Resilience Enhancement Scheme

Based on the proposed MINLP model, the optimal defending strategies of 8 states are calculated. The urgent adaption strategies are illustrated in Fig. 13 and the prevention strategies are listed in Table III. For instance, the initial strategy for state 3 does not involve switch shifting, while 163MW load curtailment and a generation rescheduling cost of $5796 are needed to guarantee transient stability. The urgent strategy of initial state 3 being adapted to future state 4 includes the switch shifting on line

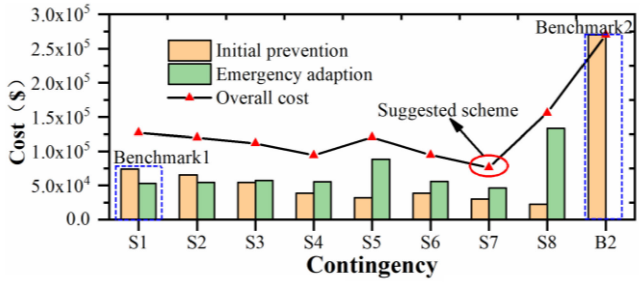

Fig. 14. Solution costs of different states.

TABLE IV
THE PREVENTION ACTION OF BENCHMARK 2

contingencies	Lines with shifted switch	Load curtailment
Scenario 1-8	L3, L6, L7, L10	537MW

14-15 to limit SCCs, 74MW load curtailment and a generation rescheduling cost of $3529 to guarantee transient stability.

Fig. 14 further illustrates the initial prevention cost, expected urgent adaption cost, as well as the overall cost of each state. As can be seen, the initial prevention cost of state 8 is the lowest while its adaption cost is the highest ($133318). Comparing the costs of state 1 and 3, it can be concluded that if fewer initial preventions are adopted, more urgent adaptions are demanded when the weather suddenly changes. The overall cost is utilized to select the optimal preventive action. The preventive action which is specially designed for state 7 achieves the lowest overall cost of $76210. Therefore, the most cost-effective strategy to defend against the uncertain hurricane is to adopt the prevention strategy under state 7 with the expected SCF on line 23–36.

D. Comparison Studies

To verify the validity of the proposed multi-state resilience enhancement method and the necessity of considering SCFs, three benchmark cases are designed as follows:

Benchmark 1: The most likely scenario with the largest occurrence probability is considered (S1 in Table II) while other possible scenarios are excluded. In this case, the suggested scheme should survive from the most probable fault.

Benchmark 2: All possible fault scenarios (S1-8 in Table II) are considered simultaneously. In this case, the suggested scheme should survive from the whole set of expected faults.

Benchmark 3: S7 is considered while its expected fault type is set as direct damage of line 23-36 but not a SCF.

The deterministic initial preventions and the urgent adaptions of benchmark 1 can be found in Table III and Fig. 13. Table IV shows the prevention actions of benchmark 2. The costs of benchmark 1 and 2 are framed in Fig. 14. The costs of benchmark 1 include $73931.70 for prevention and $53237.82 for adaption, and the total cost is $127169.52. Although the urgent adaption cost of benchmark1 is relatively low, its overall cost is higher than that of the suggested scheme (state 7). All possible scenarios are considered simultaneously in benchmark

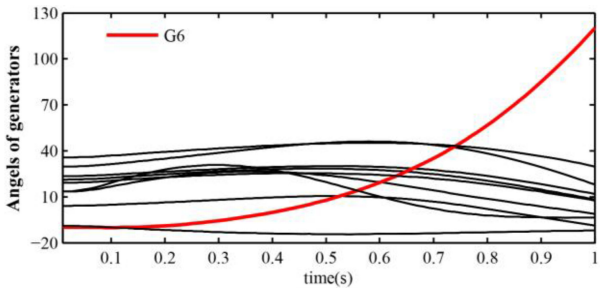

Fig. 15. Rotor angles with respect to COI in Benchmark 3.

2, therefore, there is no need for urgent adaption. In other words, the cost of preventive action is indeed the total cost with a value of $270334.24, which is highest compared with the other benchmarks. For the proposed method, initial prevention and expected urgent adaption costs are considered as the objective, which is the most economical compared with the above two benchmarks.

In benchmark 3, the rescheduling of generators with the cost of $1312 is required to ensure the security of the system in terms of the breakage of line 23-36, and no load shedding is needed. If the actual fault is a SCF in line 23-36 but not its line damage, simulations are performed to check the consequences. Firstly, the SCC is within the threshold. Meanwhile, the post-fault rotor angle of unit 6 deviates from the COI and causes transient instability, which is illustrated in Fig. 15. To guarantee transient stability, 147MW load curtailment and a generation rescheduling cost of $4926 are needed. In other words, the preventive actions considering transmission line breakages are inadequate. Therefore, it is of great necessity to consider SCFs caused by extreme weather in the resilience enhancement of power systems.

VII. Conclusion

Faced with the severe impacts of weather disasters, this paper proposed a multi-state model to determine the transmission system resilience enhancement strategy against SCFs caused by extreme weather events. Specifically, the weather-induced nodal SCF probabilities as well as grid defending measures against the out-of-range SCC magnitude and system transient instability are all integrated.

The results show that the proposed multi-state model for the transmission system resilience enhancement achieves both the increased scheme flexibility and decreased investment cost, which is easily extended to other extreme disasters, such as wildfires, line icing, etc.

References

[1] A. R. Berkeley and M. Wallace, A Framework for Establishing Critical Infrastructure Resilience Goals: Final Goals and Recommendations. Washington, DC, USA: Nat. Infrastruct. Advisory Council, Oct. 2010.

[2] D. N. Trakas and N. D. Hatziargyriou, "Optimal distribution system operation for enhancing resilience against wildfires," *IEEE Trans. Power Syst.*, vol. 33, no. 2, pp. 2260–2271, Mar. 2018.

[3] T. T. Dan and W. T. P. Wang, "A more resilient grid: The U.S. department of energy joins with stakeholders in an R&D plan," *IEEE Power Energy Mag.*, vol. 13, no. 3, pp. 26–34, May/Jun. 2015.

[4] A. Gholami, T. Shekari, F. Aminifar, and M. Shahidehpour, "Microgrid scheduling with uncertainty: The quest for resilience," *IEEE Trans. Smart Grid*, vol. 7, no. 6, pp. 2849–2858, Nov. 2016.

[5] A. Khodaei, "Resiliency-oriented microgrid optimal scheduling," *IEEE Trans. Smart Grid*, vol. 5, no. 4, pp. 1584–1591, Jul. 2014.

[6] M. Ouyang and L. Dueñas-Osorio, "Multi-dimensional hurricane resilience assessment of electric power systems," *Struct. Saf.*, vol. 48, pp. 15–24, 2014.

[7] J. P. Conti, "The day the samba stopped," *Eng. Technol.*, vol. 5, no. 4, pp. 46–47, 2010.

[8] G. Li *et al.*, "Risk analysis for distribution systems in the northeast U.S. under wind storms," *IEEE Trans. Power Syst.*, vol. 29, no. 2, pp. 889–898, Mar. 2014.

[9] P. Yu, B. Venkatesh, A. Yazdani, and B. N. Singh, "Optimal location and sizing of fault current limiters in mesh networks using iterative mixed integer nonlinear programming," *IEEE Trans. Power Syst.*, vol. 31, no. 6, pp. 4776–4783, Nov. 2016.

[10] C. Guo, C. Ye, Y. Ding, Z. Lin, and P. Wang, "Risk-based many-objective configuration of power system fault current limiters utilising NSGA-III," *IET Gener. Transmiss. Distrib.*, vol. 14, no. 23, pp. 5646–5654, 2020.

[11] C. Ye and M. Huang, "Multi-objective optimal configuration of current limiting strategies," *Sci. China Technol. Sci.*, vol. 57, no. 9, pp. 1738–1749, 2014.

[12] Y. Dong, Z. Kang, and L. Yutian, "Coordinated optimization for controlling short circuit current and multi-infeed DC interaction," *J. Modern Power Syst. Clean Energy*, vol. 2, no. 4, pp. 374–384, 2014.

[13] K. Hongesombut, Y. Mitani, and K. Tsuji, "Optimal location assignment and design of superconducting fault current limiters applied to loop power systems," *IEEE Trans. Appl. Supercond.*, vol. 13, no. 2, pp. 1828–1831, Jun. 2003.

[14] Q. Jiang and G. Geng, "A reduced-space interior point method for transient stability constrained optimal power flow," *IEEE Trans. Power Syst.*, vol. 25, no. 3, pp. 1232–1240, Aug. 2010.

[15] Y. Wang, J. Min, and Y. Chen, "Impact of the hybrid gain ensemble data assimilation on meso-scale numerical weather prediction over east China," *Atmospheric Res.*, vol. 206, pp. 30–45, 2018.

[16] W. Yuan, J. Wang, F. Qiu, C. Chen, C. Kang, and B. Zeng, "Robust optimization-based resilient distribution network planning against natural disasters," *IEEE Trans. Smart Grid*, vol. 7, no. 6, pp. 2817–2826, Nov. 2016.

[17] C. Lee, C. Liu, S. Mehrotra, and Z. Bie, "Robust distribution network reconfiguration," *IEEE Trans. Smart Grid*, vol. 6, no. 2, pp. 836–842, Mar. 2015.

[18] Z. Wang, B. Chen, J. Wang, J. Kim, and M. M. Begovic, "Robust optimization based optimal DG placement in microgrids," *IEEE Trans. Smart Grid*, vol. 5, no. 5, pp. 2173–2182, Sep. 2014.

[19] M. Agarwal *et al.*, "Optimized circuit failure prediction for aging: Practicality and promise," in *Proc. IEEE Int. Test Conf.*, 2008, pp. 1–10.

[20] M. S. Alvarez-Alvarado and D. Jayaweera, "Bathtub curve as a Markovian process to describe the reliability of repairable components," *IET Gener., Transmiss. Distrib.*, vol. 12, no. 21, pp. 5683–5689, 2018.

[21] E. Broström and L. Söder, "Modelling of ice storms for power transmission reliability calculations," in *Proc. 15th Power Syst. Comput. Conf.*, 2005, pp. 1–7.

[22] A. M. Salman, Y. Li, and M. G. Stewart, "Evaluating system reliability and targeted hardening strategies of power distribution systems subjected to hurricanes," *Rel. Eng. Syst. Saf.*, vol. 144, pp. 319–333, 2015.

[23] M. H. J. Bollen, "Effects of adverse weather and aging on power system reliability," *IEEE Trans. Ind. Appl.*, vol. 37, no. 2, pp. 452–457, Mar./Apr. 2001.

[24] D. P. Kothari and I. J. Nagrath, *Modern Power System Analysis*, 3rd ed., New Delhi, India: TATA McGraw-Hill, 2003.

[25] J. H. Teng and C. N. Lu, "Optimum fault current limiter placement with search space reduction technique," *IET Gener. Transmiss. Distrib.*, vol. 4, no. 4, pp. 485–494, 2010.

[26] L. Tang, W. Tang, X. Chang, S. Miao, L. Wang, and X. Yuan, "Network connectivity identification method based on incidence matrix and branch pointer vector," in *Proc. IEEE Innov. Smart Grid Technol.-Asia*, Chengdu, China, 2019, pp. 429–433.

[27] D. Gan, R. J. Thomas, and R. D. Zimmerman, "Stability-constrained optimal power flow," *IEEE Trans. Power Syst.*, vol. 15, no. 2, pp. 535–540, May 2000.

[28] G. J. Alaka Jr., X. Zhang, S. G. Gopalakrishnan, Z. Zhang, F. D. Marks, and R. Atlas, "Track uncertainty in high-resolution HWRF ensemble forecasts of hurricane joaquin," *Weather Forecasting*, vol. 34, no. 6, pp. 1889–1908, 2019.
[29] A. T. Hazelton, M. Bender, M. Morin, L. Harris, and S.-J. Lin, "2017 Atlantic hurricane forecasts from a high-resolution version of the GFDL fvGFS model: Evaluation of track, intensity, and structure," *Weather Forecasting*, vol. 33, no. 5, pp. 1317–1337, 2018.
[30] Burma Cyclone was Forecast Four Days in Advance. 2008. [Online]. Available: https://www.newscientist.com/article/dn13868-burma-cyclone-was-forecast-four-days-in-advance/
[31] Z. Wang, X. Song, H. Xin, D. Gan, and K. P. Wong, "Risk-based coordination of generation rescheduling and load shedding for transient stability enhancement," *IEEE Trans. Power Syst.*, vol. 28, no. 4, pp. 4674–4682, Nov. 2013.
[32] C.-J. Ye and M.-X. Huang, "Multi-objective optimal power flow considering transient stability based on parallel NSGA-II," *IEEE Trans. Power Syst.*, vol. 30, no. 2, pp. 857–866, Mar. 2014.
[33] L. Chen, M. Huang, J. Wu, and D. Wang, "An optimal strategy for short circuit current limiter deployment," in *Asia-Pacific Power Energy Eng. Conf.*, Chengdu, 2010, pp. 1–4.
[34] China Weather Hurricane Network, China Climate Network, 2020. [Online]. Available: http://typhoon.weather.com.cn/

Chao Guo received the B.S. degree in electrical engineering from Shandong University, Jinan, China. He is currently working toward the Ph.D. degree in electric engineering from Zhejiang University, Hangzhou, China. His research interests include reliability analysis, short-circuit current limitation, and the power market.

Chengjin Ye received the B.E. and Ph.D. degrees in electrical engineering from Zhejiang University, Hangzhou, China, in 2010 and 2015, respectively. From 2015 to 2017, he was a Distribution System Engineer with the Economics Institute of State Grid Zhejiang Electric Power Company, Ltd. From 2017 to 2019, he was a Postdoc Researcher with Zhejiang University. Since 2020, he has been a Research Professor with the College of Electrical Engineering, Zhejiang University. His research interests include data-driven power system planning and operation, short-circuit current limitation, and integration of demand side resources into power system operation.

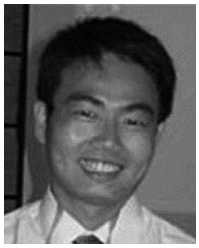

Yi Ding (Member, IEEE) received the bachelor's degree in electrical engineering from Shanghai Jiaotong University, Shanghai, China, and the Ph.D. degree in electrical engineering from Nanyang Technological University, Singapore, in 2002 and 2007, respectively. He is currently a Professor with the College of Electrical Engineering, Zhejiang University, Hangzhou, China. His current research interests include power systems reliability analysis incorporating renewable energy resources, smart grid performance analysis, and engineering systems reliability modeling and optimization.

Peng Wang (Fellow, IEEE) received the Ph.D. degree from the University of Saskatchewan, Saskatoon, SK, Canada. He is currently a Professor with Electrical and Electronic Engineering School, Nanyang Technological University, Singapore. His research interests include power system planning and operation, renewable energy planning, solar/electricity conversion systems, power market, and power system reliability analysis.